

RESEARCH

Open Access



DCE-MRI radiomics of primary breast lesions combined with ipsilateral axillary lymph nodes for predicting efficacy of NAT

Yiyao Sun^{1†}, Qingxuan Liao^{1†}, Ying Fan^{2†}, Chunxiao Cui³, Yan Wang¹, Chunna Yang¹, Yang Hou^{4*} and Dan Zhao^{5*}

Abstract

Background This study aimed to assess the predictive value of radiomic analysis derived from primary lesions and ipsilateral axillary suspicious lymph nodes (SLN) on dynamic contrast-enhanced MRI (DCE-MRI) for evaluating the response to neoadjuvant therapy (NAT) in early high-risk and advanced breast cancer (BC) patients.

Methods A retrospective analysis was conducted on 222 BC patients (192 from Center I and 30 from Center II) who underwent NAT. Radiomic features were extracted from the primary lesion (intra- and peritumoral regions) and ipsilateral axillary SLN to develop radiomic signatures (RS-primary, RS-SLN). An integrated signature (RS-Com) combined features from both regions. Feature selection was performed using correlation analysis, the Mann-Whitney U test, and least absolute shrinkage and selection operator (LASSO) regression. A diagnostic nomogram was constructed by integrating RS-Com with key clinical factors. Model performance was evaluated using receiver operating characteristic (ROC) and decision curve analysis (DCA).

Results RS-Com demonstrated superior predictive performance compared to RS-primary and RS-SLN alone. The DeLong test confirmed that axillary SLNs provide supplementary information to the primary lesion. Among clinical factors, N staging and HER2 status were significant contributors. The nomogram, integrating RS-Com, N staging, and HER2 status, achieved the highest performance in the training (AUC: 0.926), validation (AUC: 0.868), and test (AUC: 0.839) cohorts, outperforming both the clinical models and RS-Com alone.

Conclusion Radiomic features from axillary SLNs offer valuable supplementary information for predicting NAT response in BC patients. The proposed nomogram, incorporating radiomics and clinical factors, provides a robust tool for individualized treatment planning.

Keywords Breast cancer, Neoadjuvant therapy, Radiomics, MRI

[†]Yiyao Sun, Qingxuan Liao and Ying Fan contributed equally to this work and share first authorship.

*Correspondence:

Yang Hou
houyang1973@163.com
Dan Zhao
zhaodan777@126.com

¹School of Intelligent Medicine, China Medical University, Shenyang, Liaoning 110122, P.R. China

²Department of Biomedical Engineering, School of Information Science and Technology, Fudan University, Shanghai 200082, P.R. China

³Department of Breast Imaging, Affiliated Hospital of Qingdao University, Qingdao, Shandong 266100, P.R. China

⁴Department of Radiology, Shengjing Hospital of China Medical University, Shenyang, Liaoning 110004, P.R. China

⁵Department of Medical Imaging, Liaoning Cancer Hospital & Institute, Shenyang, Liaoning 110042, P.R. China



Introduction

Breast cancer (BC) is the most common malignancy in women worldwide [1], with around 40% of advanced-stage initial diagnoses found to harbor ipsilateral axillary suspicious lymph nodes (SLNs) [2]. Currently, the preferred treatment for early high-risk BC and locally advanced BC is neoadjuvant therapy (NAT) [3], referring to a series of systemic treatments received prior to surgery, which include neoadjuvant chemotherapy, targeted therapy, endocrine therapy and radiotherapy [4].

The pathological assessment systems after NAT include the Miller-Payne (MP) system, the Residual Cancer Burden (RCB) system, and the American Joint Committee on Cancer (AJCC) ypTNM staging system [5, 6]. The MP system, commonly used in pathology, primarily evaluates the cellularity of residual tumors in the primary breast lesion after neoadjuvant therapy [7]. Previous studies have indicated that patients who achieve a G4 or G5 pathological response have a 5-year survival rate of 81% and 100%, respectively [8]. Achieving a G4-G5 response post-NAT indicates sensitivity to treatment, making breast-conserving surgery feasible, with overall good survival and prognosis for these patients [9]. As a surrogate endpoint for prediction of long-term prognostication, G4-5 has been expected to be achieved after NAT, which are independent predictors of response to NAT and favorable prognosis [10]. Therefore, there is an urgent need to develop an effective predictive method to accurately identify G4-5 patients before NAT. Dynamic contrast-enhanced magnetic resonance imaging (DCE-MRI) is capable of providing morphological characteristics of tumors, offers insights into tumor perfusion and hemodynamic features [11], and thus is the preferred imaging modality in evaluating the efficiency of NAT [12]. However, radiologists can hardly determine which patients will benefit from NAT by visual inspection of breast DCE-MRI, because there is still no specific marker.

Radiomic analysis involves the high-throughput extraction of quantitative imaging features, which characterize the spatial relationships and consistency of signal intensities [13]. Compared to tissue biopsies, radiomics inherits the non-invasive and repeatable technical advantages of imaging examinations, providing a safer and more reliable technical approach for patient follow-up and prognosis. Radiomic analysis based on DCE-MRI has been proven effective in predicting various biological aspects of BC, which include prediction of receptor status [14], subtypes [15], and genomics [16]. Previous works have demonstrated that the radiomics is capable of predicting post-treatment response to NAT in BC patients [17]. Previous studies generally focus on the primary tumor site [18, 19] or combine the peritumoral region [20, 21] for radiomic analysis. The results highlight the importance of the tumor microenvironment in developing predictive

models for early prediction of treatment response and outcomes. However, published works only focused on the primary lesion, and ignored the potential value of ipsilateral axillary SLN diagnosed by baseline MRI.

Emerging evidence indicates that the tumor microenvironment in close proximity to the tumor may contain additional valuable information, such as angiogenesis [22], stromal response [23], and lymphangiogenesis [24] activities. This can lead to morphological and structural changes in SLN, exhibiting varying degrees of heterogeneity. Consequently, analyzing only primary lesions would neglect crucial information regarding the microenvironment of SLN, given the intricate interplay between peripheral breast and lymphoid tissues [25]. Therefore, to capture full information contained in MRI data, analysis should not be limited to the primary lesion but should also include the SLN regions.

This study aims to explore predictive value of radiomic features from both primary lesion and ipsilateral axillary SLN diagnosed by baseline MRI, then evaluate the feasibility of utilizing a radiomics-clinical nomogram based on primary lesion, ipsilateral axillary SLNs and important clinical factors for predicting response following NAT in high-risk early-stage and locally advanced breast cancer (LABC).

Methods

Patients

We retrospectively collected 192 cases from Center 1 (between March 2018 and December 2022) and 30 cases from Center 2 (between July 2021 and February 2023) on female BC patients who were pathologically diagnosed and underwent NAT before surgery. Patients who underwent NAT were grouped using the Miller-Payne grading system. Patients with MP grades G1-3 were classified as the NAT-low response group, while those with MP grades G4-5 were classified as the NAT-high response group [8].

In this study, all core needle biopsy and postoperative specimens underwent pathological hematoxylin and eosin (HE) staining as well as immunohistochemical (IHC) analysis. Estrogen receptor (ER) and progesterone receptor (PR) were considered positive if their expression was $\geq 1\%$ and negative if $< 1\%$. Ki-67 was classified as positive if $\geq 30\%$ and negative if $< 30\%$ [26]. For the evaluation of HER2 expression in breast cancer specimens, initial IHC testing was performed: IHC 3+ was defined as positive, while IHC 0 and 1+ were considered negative. Specimens with IHC 2+ required further fluorescence in situ hybridization (FISH) testing; a positive FISH result was defined as HER2-positive, whereas a negative FISH result was defined as HER2-negative [26]. The N staging refers to clinical staging (cN). Clinical N staging is primarily determined through physical examination by

clinicians and radiological assessments, including imaging methods such as ultrasound and MRI, to evaluate the size and characteristics of the axillary lymph nodes before treatment [27]. It indicates lymph node involvement: N0 indicates no regional lymph node metastasis; N1 indicates ipsilateral axillary lymph node metastasis, but the lymph nodes are mobile; N2 indicates metastasis in ipsilateral axillary lymph node, fixed or matted. Or ipsilateral internal mammary lymph node metastasis; N3 indicates ipsilateral infraclavicular lymph node metastasis, or ipsilateral internal mammary and axillary lymph node metastasis, or ipsilateral supraclavicular lymph node metastasis.

The inclusion criteria are as follows: (1) Patients with clinical stage I-III BC; (2) Patients with initially diagnosed primary unilateral BC, without distant metastasis, and no history of surgery or other BC treatments; (3) Patients who received at least four cycles of NAT and underwent surgery after the completion of NAT; (4) Patients who underwent breast DCE-MRI and ultrasound examinations before NAT; (5) Patients with ipsilateral axillary positive lymph nodes before NAT, diagnosed comprehensively by DCE-MRI and ultrasound; (6) Complete pathological data from post-surgical and pre-NAT biopsy; and (7) Pathological type: invasive ductal carcinoma. The exclusion criteria are as follows: (1) Patients with bilateral BC; (2) Patients with distant metastasis or a history of other malignant tumors; and (3) Incomplete pathological, clinical, or imaging data, or inability to follow up. Patients from Center I ($n=192$) were divided into training and validation sets in a ratio of 2:1. Patients from Center II ($n=30$) were used to independently test the models. Figure 1 depicts a flowchart of the patients included in this study. Figure 2 depicts a flowchart of the patient inclusion and exclusion.

MRI image acquisition

Pre-treatment DCE-MRI scans were performed within one week prior to NAT treatment. All enrolled cases underwent contrast-enhanced breast MRI scans before NAT. For the DCE-MRI scans, Center I utilized a GE 1.5T superconducting MRI scanner, while Center II employed both SIEMENS 3.0T and GE 3.0T superconducting MRI scanners. After contrast administration, Center I's GE 1.5T MRI collected continuous data for 8 consecutive scans without intervals, Center II's SIEMENS 3.0T MRI collected continuous data for 5 consecutive scans without intervals, and Center II's GE 3.0T MRI collected continuous data for 5 consecutive scans without intervals. The detailed MRI sequence parameters can be found in the Supplementary Materials (Appendix A). All images were downloaded and analyzed in DICOM format from the PACS system.

ROI segmentation

The region of interest (ROI) corresponding to the entire tumor and ipsilateral axillary SLN was delineated slice-by-slice on DCE-MRI (peak phase) images by a radiologist (AA) with 5 years of experience, utilizing ITK-SNAP (version 4.0.1). The ROIs encompassed the entirety of the primary tumor region and ipsilateral axillary SLN. In this experiment, when multiple SLNs are present, the imaging of the SLN with the maximum short-axis diameter is used [28]. Underwent validation by a senior radiologist (AA) with 15 years of professional experience. The ROI of the peritumoral area surrounding the tumor (peritumoral ROI) were derived from manually delineated ROIs. To achieve this, the original ROIs were radially expanded to 4 millimeters [29] outside the tumor with Python (v.3.7), resulting in the creation of dilated ROIs. Figure 3 illustrates the generated ROIs of the primary lesion and ipsilateral axillary SLN in the MRI image.

Feature extraction and selection

The Pyradiomics software package [30] (<https://pyradiomics.readthedocs.io/en/v3.0.1/>) was employed to compute radiomic features from the tumor region, peritumoral region and ipsilateral axillary SLN. Features were extracted from the original peak-phase DCE-MRI images [31], encompassing first-order, shape-based (2D/3D), and textural features. Furthermore, detailed descriptions of post-filtering features are provided in the Pyradiomics documentation. Subsequently, a total of 5901 ($1967 \times 3 = 5901$) features were extracted for each patient across three locations, encompassing features from both intra- and peritumoral regions ($1967 \times 2 = 3934$), as well as ipsilateral axillary SLN ($1967 \times 1 = 1967$). Each set of extracted features underwent the following procedures: firstly, intraclass correlation coefficient (ICC) analysis was performed on the features, retaining those with ICC values exceeding 0.85 [32], the detailed ICC content can be found in Appendix C of the Supplementary Materials. Then, the Mann-Whitney U test was applied to compare the features between two patient groups, which were defined based on their response to NAT: NAT-low (patients with MP grades G1-3) and NAT-high (patients with MP grades G4-5). Features with a p-value greater than 0.05 were considered statistically insignificant and discarded. Lastly, the least absolute shrinkage and selection operator (LASSO) regression with 10-fold cross-validation was carried out using the glmnet package in R (version 3.6.1, Boston, MA, USA).

Construction of radiomics model and clinical model

The LASSO method was used for the preliminary feature selection of RS from the primary lesion and ipsilateral axillary SLN. To address the issue of feature collinearity,

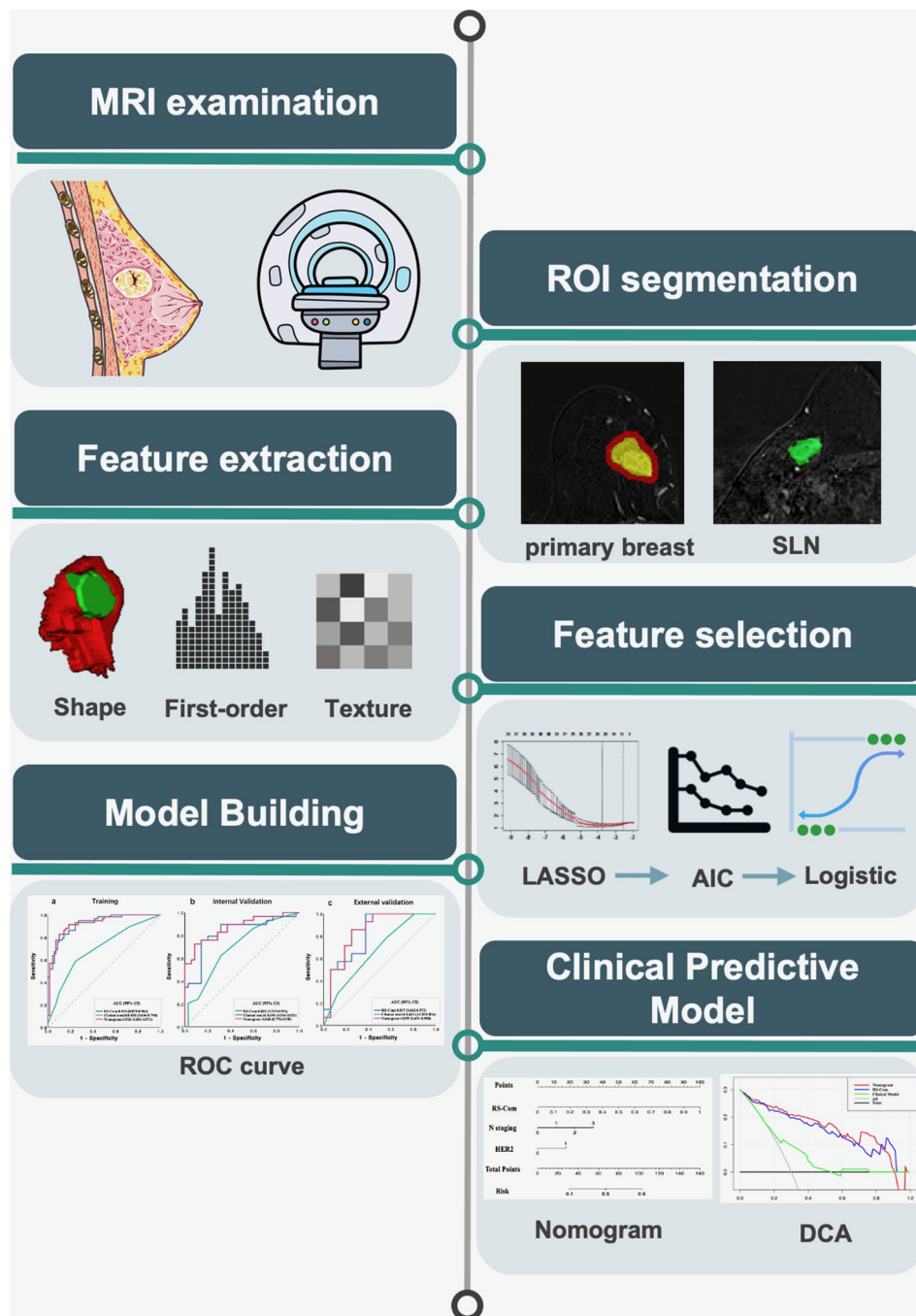


Fig. 1 Diagram of the study design for predicting efficacy of NAT

the variance inflation factor (VIF) was evaluated. The goodness-of-fit of the model was assessed using the Hosmer-Lemeshow test and calibration curve analysis. Subsequently, backward stepwise elimination based on the Akaike Information Criterion (AIC) was applied to remove redundant features and enhance model fitting [33]. Finally, logistic regression was used to assign weights to the model and construct a clinical model incorporating the most critical clinical factors, which

were selected based on their statistical significance (p -value less than 0.05) and clinical relevance. These factors were identified through an initial univariate analysis followed by multivariate regression to ensure that only the most impactful variables were included in the final model [34]. The Spearman rank correlation coefficient was used to test the correlation between features [35]. Features with a correlation coefficient greater than 0.7 were considered correlated and removed. A diagnostic

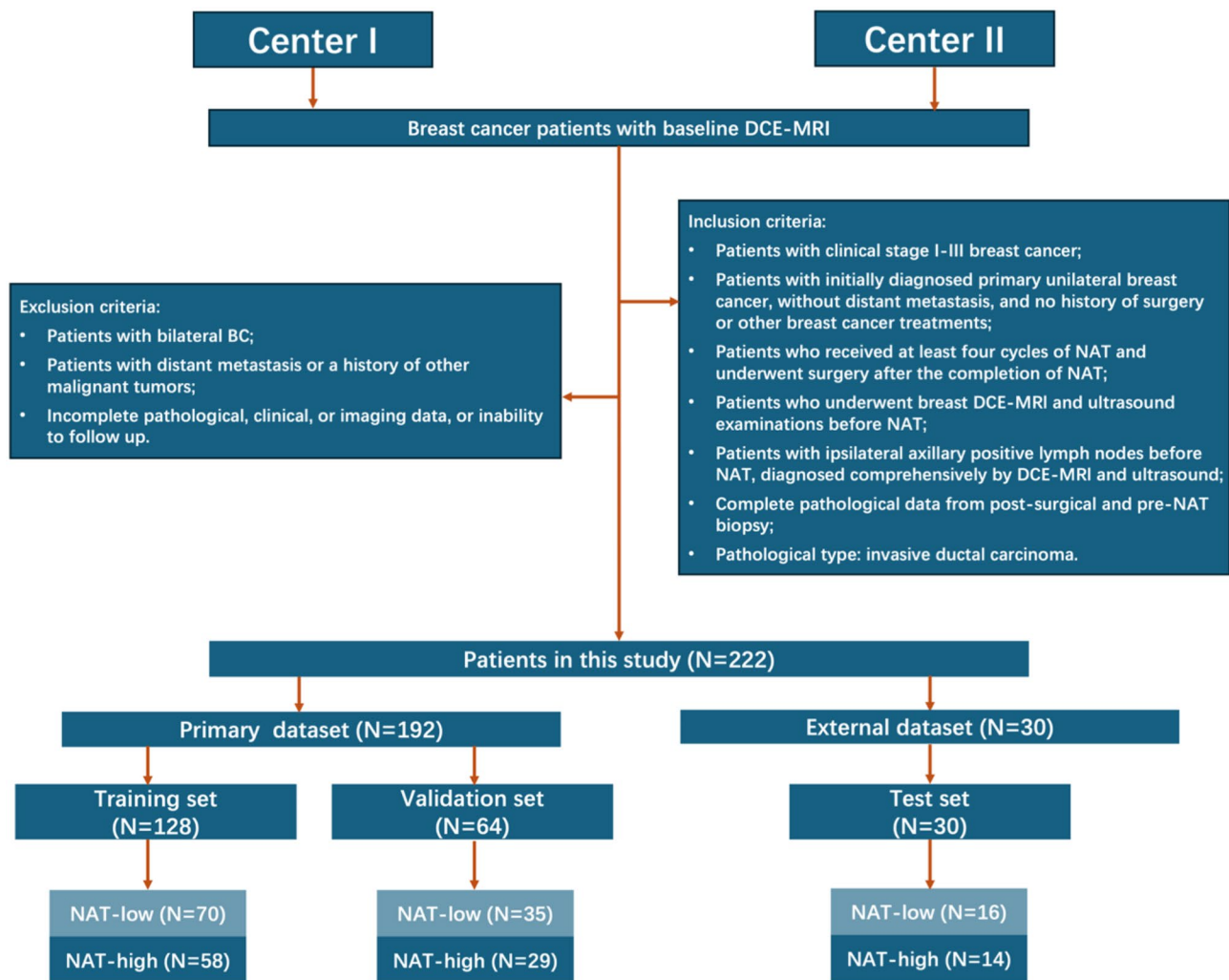


Fig. 2 Flowchart of the patient inclusion and exclusion

nomogram model incorporating the radiomic signatures and clinical factors was constructed using the rms package in R [36].

Outcomes

The primary outcome of this study was to assess the ability of the radiomics model to predict the response to NAT in BC patients using features from DCE-MRI. The model's performance was evaluated based on accuracy (ACC), sensitivity (SEN), specificity (SPE), and area under the receiver operating characteristic curve (AUC) across the training, validation, and test cohorts. A secondary outcome was the development and validation of a nomogram combining the model's results with key clinical factors. The nomogram's performance was evaluated for its predictive accuracy and clinical decision-making support. Additionally, subgroup analyses were performed to assess the model's performance in HER2-positive and HER2-negative patients, aiming to explore how HER2

status impacts the response to NAT and enhance the model's clinical applicability for personalized treatment.

Statistical analysis

Statistical analysis was performed using SPSS software (version 26.0, Chicago, IL) and R software. The normality and homogeneity of variance assumptions were assessed using the Kolmogorov-Smirnov test and Bartlett test, respectively. Quantitative data were analyzed using independent samples t-test or Mann-Whitney *U* test, while categorical data were analyzed using chi-square test or Fisher exact test. Receiver operating characteristic (ROC) curves were plotted, and optimal cutoff values were determined using the maximum Youden index [37]. Subsequently, the area under the ROC curve (AUC) was calculated to evaluate model performance. DeLong's test was utilized for statistical comparisons of each model [38]. For nested models, we used the likelihood ratio test (LRT) to assess AUC differences [39]. To

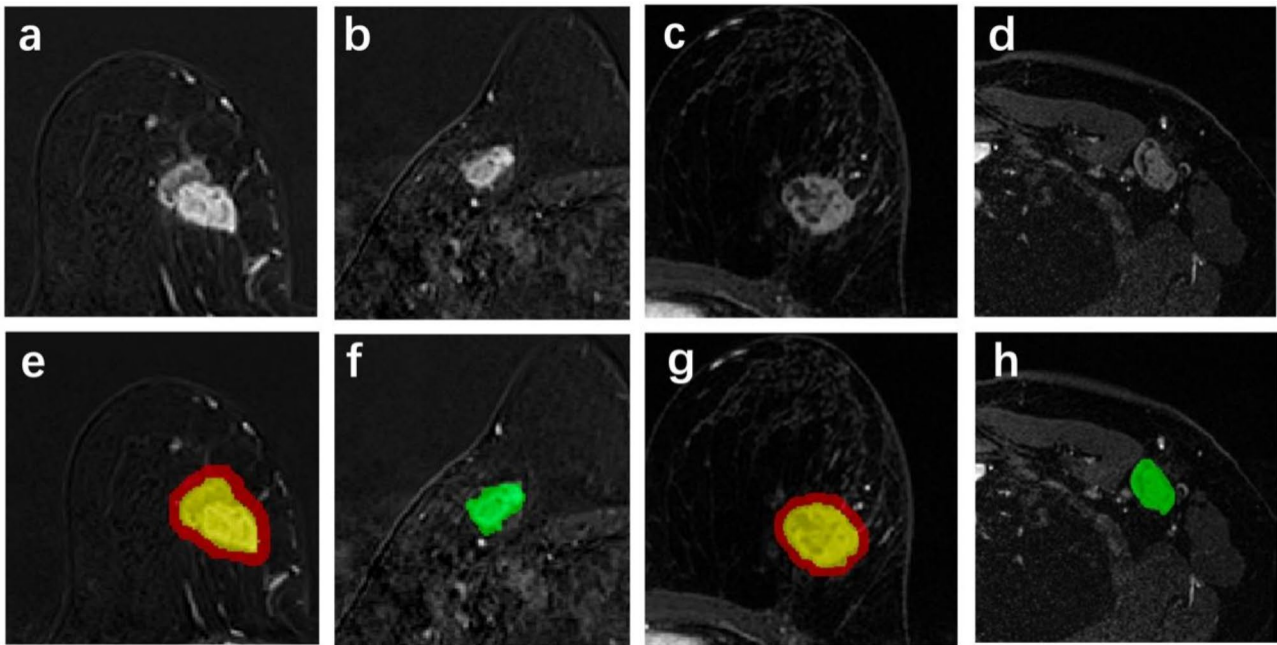


Fig. 3 Examples of generated ROIs delineating the primary lesion and ipsilateral axillary SLN in MRI images. Panels (a, b, e, and f) show a 59-year-old patient with NAT-low, featuring the primary lesion (a, e) and ipsilateral axillary SLN (b, f). Panels (c, d, g, and h) depict a 41-year-old patient with NAT-high, illustrating the primary lesion (c, g) and SLN (d, h). The yellow regions represent manually delineated tumor ROIs covering the entire tumor, while the red regions indicate peritumoral ROIs. The green regions show manually delineated ROIs of the ipsilateral axillary SLN

assess the clinical utility of the models, decision curve analysis (DCA) was applied, and net benefits for a range of threshold probabilities were computed using the *rmda* package in R. All tests were two-tailed, and $p < 0.05$ was considered statistically significant.

Results

Patient characteristics

Table 1 shows the patients' statistical analysis of the clinical characteristics, including age, clinical T stage, clinical N stage, ER status, PR status, HER2 status, Ki67 status, and MP grade. N staging and HER2 status were significantly associated with response to NAT ($p < 0.05$) in both primary and external cohorts. Age, T staging, ER, PR, and Ki-67 were found to be not significantly different ($P > 0.05$). The exact p values of each characteristic were listed in Table 1.

Features selection and RS development

Radiomic features were extracted from both primary lesion (tumor and peritumoral regions) and ipsilateral axillary SLN. Supplementary Figure S1 presents selection of features relevant to NAT responses using LASSO. Table 2 details performances of each selected feature.

Among the selected features, seven were derived from the primary lesion, including three from the tumor region and four from the peritumoral region. Additionally, three features were derived from the ipsilateral axillary SLN region. The optimal sets of features identified from primary lesion and ipsilateral axillary SLN were used to construct radiomic signatures (RSs) named RS-Primary and RS-SLN, respectively. The combined RS (RS-Com) was developed integrating the most predictive features from primary lesion and ipsilateral axillary SLN. The formula for RS, which integrates the features with their corresponding coefficients, can be found in the Supplementary Materials (Appendix B). The Spearman rank correlation coefficient results (Figure S2) show that there is no correlation among the final features.

Evaluation of the developed RSs

As shown in Table 3, the developed RS derived from ipsilateral axillary SLN (RS-SLN) demonstrated the lowest accuracy. The RS derived from primary lesion (RS-primary) outperformed RS-SLN with regards to AUC, ACC, SPE and SEN. By integrating features from both SLN and primary lesion, the combined model (RS-Com) generated the highest AUC, ACC and SPE. More importantly, we

Table 1 Characteristics for all patients from primary and external cohorts

Characteristic	Training cohort (n = 128)		P	Validation cohort (n = 64)		P	Test cohort (n = 30)		P
	NAT-low (n = 70)	NAT-high (n = 58)		NAT-low (n = 35)	NAT-high (n = 29)		NAT-low (n = 16)	NAT-high (n = 14)	
Age, year (Mean ± SD)	51.34 ± 10.92	53.03 ± 10.17	0.488	53.59 ± 8.95	51.26 ± 10.66	0.206	47.41 ± 8.93	48.50 ± 9.44	0.892
T staging, No (%)			0.192			0.184			0.126
T1	3 (4.28)	4 (6.89)		2 (88.24)	1 (3.44)		0 (0.00)	1 (7.14)	
T2	54 (77.14)	49 (84.48)		26 (11.76)	25 (86.20)		13 (81.25)	11 (78.57)	
T3	5 (71.42)	2 (3.44)		3 (8.57)	2 (6.89)		1 (6.25)	0 (0.00)	
T4	8 (11.42)	3 (5.17)		4 (1.42)	1 (3.44)		2 (12.50)	2 (14.28)	
N staging, No (%)			0.012*			0.039*			0.046*
N0	21 (30.00)	7 (12.06)		14 (40.00)	4 (13.79)		7 (43.75)	2 (14.28)	
N1	42 (60.00)	33 (56.89)		17 (48.57)	18 (62.06)		7 (43.75)	6 (42.85)	
N2	7 (10.00)	16 (27.58)		3 (8.57)	7 (24.13)		2 (12.50)	6 (42.85)	
N3	0 (0.00)	2 (3.44)		1 (2.85)	0 (0.00)		0 (0.00)	0 (0.00)	
ER, No (%)			0.102			0.079			0.154
Positive	48 (68.57)	30 (51.72)		21 (60.00)	17 (58.62)		12 (75.00)	9 (64.28)	
Negative	22 (31.42)	28 (48.27)		14 (40.00)	12 (41.37)		4 (25.00)	5 (35.71)	
PR, No (%)			0.066			0.143			0.169
Positive	41 (58.57)	23 (39.65)		23 (65.71)	13 (44.82)		11 (68.75)	9 (64.28)	
Negative	29 (41.42)	35 (60.34)		12 (34.28)	16 (55.17)		5 (31.25)	5 (35.71)	
HER2, No (%)			0.013*			0.050*			0.048*
Positive	17 (24.28)	29 (50.00)		13 (52.00)	19 (65.51)		6 (37.50)	11 (78.57)	
Negative	53 (75.71)	29 (50.00)		22 (62.85)	10 (34.48)		10 (62.50)	3 (21.42)	
Ki-67, No (%)			0.078			0.043*			0.169
Positive	42 (70.00)	50 (86.20)		29 (82.85)	22 (75.86)		11 (68.75)	9 (64.28)	
Negative	18 (30.00)	8 (13.80)		6 (17.15)	7 (24.14)		5 (31.25)	5 (35.72)	
MP, No (%)			<0.001*			<0.001*			<0.001*
G1	0 (0.00)	0 (0.00)		0 (0.00)	0 (0.00)		0 (0.00)	0 (0.00)	
G2	16 (22.86)	0 (0.00)		5 (14.29)	0 (0.00)		5 (31.25)	0 (0.00)	
G3	54 (77.14)	0 (0.00)		30 (85.71)	0 (0.00)		11 (68.75)	0 (0.00)	
G4	0 (0.00)	18 (31.03)		0 (0.00)	14 (48.27)		0 (0.00)	4 (28.57)	
G5	0 (0.00)	40 (68.96)		0 (0.00)	15 (51.72)		0 (0.00)	10 (71.42)	

MP, Miller-Payne; ER, Estrogen Receptor; PR, Progesterone Receptor; HER2, Human Epidermal Growth Factor Receptor 2. * $P < 0.05$

found that in the Delong test of RS-Primary vs. RS-SLN, the p -values were all less than 0.05, indicating significant differences between the feature information based on the primary lesion region and the SLN region. This suggests that SLN provides supplementary information to the primary lesion of BC, thereby enhancing the overall predictive capability (from 0.841 to 0.918). ROC curves of each RS were shown in Fig. 4. Table 4 presents the results of the subgroup analysis for HER2-positive and HER2-negative patients. The results show that the AUC and ACC for HER2-positive patients are higher than those for HER2-negative patients in the RS-primary and RS-com

models, but no significant difference was observed in the RS-SLN model.

Establishment and validation of radiomics nomogram

N staging and HER2 were identified to be predictive on response to NAT according to the smallest AIC information statistics ($p < 0.05$) in both primary and external cohorts. A clinical-radiomics nomogram was established by integrating RS-Com, N staging and HER2 (Fig. 5a). Values of each predictor (RS-Com, N staging and HER2) were mapped to the “Point” axis and can be converted to “Total Point”. The sum of the points of the predictors

Table 2 Performance of the selected features from the primary lesion and ipsilateral axillary SLN

Feature	Region	Cohort	Mean \pm SD		AUC	P
			low	high		
log.sigma.3.0.mm.3D_glcm_lmc2 (F1)	Tumor	Training	0.76 \pm 0.07	0.72 \pm 0.10	0.639	0.012*
		Validation	0.77 \pm 0.08	0.73 \pm 0.10	0.610	0.133
		Test	0.83 \pm 0.10	0.77 \pm 0.02	0.875	<0.001
log.sigma.5.0.mm.3D_glcm_InverseVariance (F2)	Tumor	Training	0.42 \pm 0.05	0.40 \pm 0.07	0.606	0.039*
		Validation	0.40 \pm 0.06	0.39 \pm 0.07	0.542	0.433
		Test	0.45 \pm 0.07	0.44 \pm 0.11	0.545	0.112
original_shape_Elongation (F3)	Tumor	Training	0.80 \pm 0.09	0.74 \pm 0.13	0.634	0.009
		Validation	0.82 \pm 0.10	0.74 \pm 0.14	0.687	0.011*
		Test	0.79 \pm 0.12	0.72 \pm 0.13	0.674	0.105
exponential_glrIm_RunVariance (F4)	Peritumoral	Training	10.75 \pm 4.36	9.17 \pm 1.52	0.696	<0.001*
		Validation	10.79 \pm 3.70	9.10 \pm 1.36	0.667	0.022*
		Test	11.07 \pm 2.94	12.35 \pm 4.38	0.567	0.467
logarithm_glcm_Correlation (F5)	Peritumoral	Training	0.56 \pm 0.11	0.51 \pm 0.10	0.626	0.014*
		Validation	0.58 \pm 0.11	0.53 \pm 0.12	0.602	0.163
		Test	0.56 \pm 0.15	0.56 \pm 0.12	0.522	0.165
wavelet.HLH_glcm_Correlation(F6)	Peritumoral	Training	0.03 \pm 0.02	0.04 \pm 0.02	0.607	0.038*
		Validation	0.03 \pm 0.02	0.03 \pm 0.03	0.510	0.113
		Test	0.06 \pm 0.04	0.12 \pm 0.06	0.830	0.002*
wavelet.LHL_glszm_SmallAreaEmphasis (F7)	Peritumoral	Training	0.42 \pm 0.04	0.41 \pm 0.04	0.616	0.024*
		Validation	0.43 \pm 0.04	0.41 \pm 0.05	0.610	0.133
		Test	0.51 \pm 0.10	0.58 \pm 0.07	0.701	0.061
lbp.3D.k_gldm_DependenceEntropy (F8)	SLN	Training	3.91 \pm 0.34	4.11 \pm 0.27	0.660	0.002*
		Validation	3.97 \pm 0.32	4.14 \pm 0.23	0.677	0.015*
		Test	3.95 \pm 0.33	4.1 \pm 0.27	0.638	0.198
wavelet.LHH_gldm_SmallDependenceLowGrayLevelEmphasis (F9)	SLN	Training	0.00 \pm 0.00	0.01 \pm 0.00	0.619	0.020
		Validation	0.00 \pm 0.00	0.01 \pm 0.00	0.659	0.029*
		Test	0.00 \pm 0.00	0.01 \pm 0.01	0.612	0.299
wavelet.HLH_glcm_lmc1 (F10)	SLN	Training	0.08 \pm 0.04	0.07 \pm 0.02	0.632	<0.001*
		Validation	0.08 \pm 0.01	0.07 \pm 0.03	0.544	0.397
		Test	0.08 \pm 0.02	0.07 \pm 0.05	0.631	0.240

SLN, suspicious lymph node; SD, standard deviation. * $P < 0.05$

indicated response to NAT. Calibration curves showed good agreements between actual probabilities and nomogram estimated probabilities (Fig. 5b–d) in primary and external sets.

As shown in Table 5, the RS-Com outperformed the clinical model in terms of AUC and ACC in both primary and external validation cohorts. The nomogram showed improved AUC and ACC compared with RS-Com and clinical model. Figure 6 depicts ROC curves of the developed nomogram, RS-Com and clinical model. DCA curves (Fig. 7) indicate that the nomogram proposed in this study will be more beneficial than RS-Com and clinical model across most threshold probabilities.

Discussion

In this study, the peak phase of the DCE-MRI sequence was employed as the optimal contrast period to capture key features of the primary tumor. Information from ipsilateral axillary SLNs was then integrated to provide additional predictive insights, contributing to the effective prediction of NAT outcomes. Finally, the nomogram, incorporating radiomic features along with HER2 status and N stage, demonstrated good calibration and predictive value across primary and external cohorts (AUC: 0.926–0.839), highlighting its generalizability and robustness in predicting various NAT responses.

Table 3 Performance of the established RSs based on primary lesion and SLN, and their combination

Model	Training cohort			Validation cohort			Test cohort			P
	AUC (95% CI)	ACC	SPE	AUC (95% CI)	ACC	SPE	AUC (95% CI)	ACC	SPE	
RS-Primary	0.841 (0.774–0.908)	0.750	0.800	0.788 (0.643–0.884)	0.688	0.828	0.746 (0.565–0.926)	0.664	0.677	0.880
RS-SLN	0.716 (0.628–0.805)	0.656	0.714	0.621 (0.540–0.810)	0.578	0.600	0.647 (0.556–0.850)	0.633	0.625	0.929
RS-Corn	0.918 (0.873–0.964)	0.815	0.757	0.822 (0.712–0.932)	0.781	0.857	0.817 (0.662–0.972)	0.733	0.625	0.946
RS- Primary vs. RS-SLN			0.009*							0.002*
RS-Corn vs. RS- Primary			< 0.001*							0.037*
RS-Corn vs. RS-SLN			0.297							0.168

AUC, area under the receiver operating characteristic curve; CI, confidence interval; ACC, accuracy; SEN, sensitivity; SPE, specificity; SLN, suspicious lymph node. *P<0.05

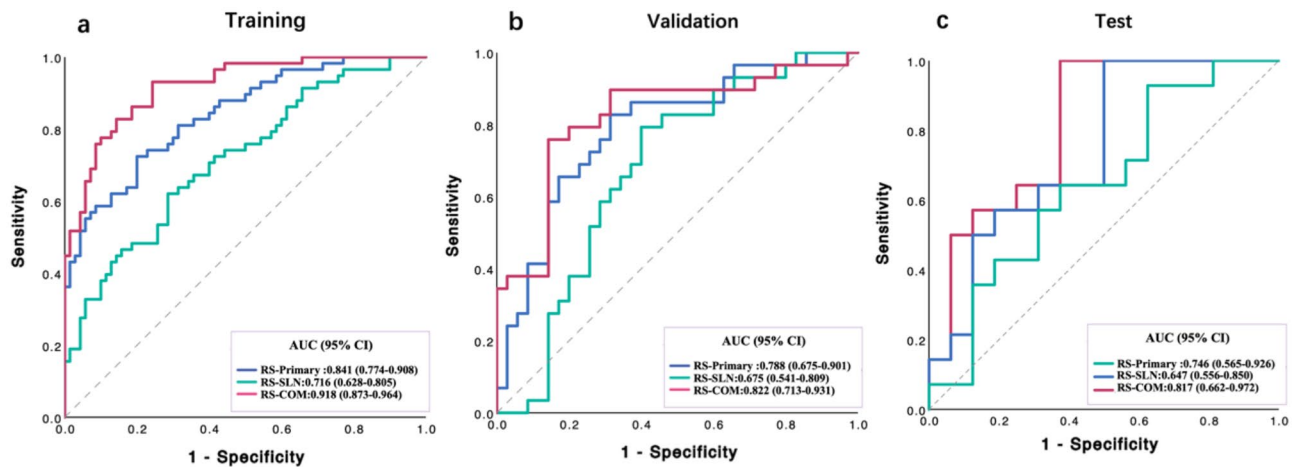


Fig. 4 Receiver operating characteristic (ROC) curves of the RSs derived from primary lesion, SLN and in combination for predicting response to NAT in training (a), validation (b) and test (c) sets

DCE-MRI, in addition to providing morphological characteristics of tumors, can also offer insights into tumor perfusion and hemodynamic properties, making it one of the most sensitive modalities for breast disease detection [40]. Although numerous studies [41, 42] have demonstrated that radiomic features derived from DCE-MRI can effectively predict the efficacy of NAT in BC, most of these studies are small-scale retrospective analyses, lacking a standardized approach for selecting enhancement time points and scanning sequences. This study selected the peak phase as the research period primarily because it provides the clearest visualization of both the primary breast lesion and suspicious lymph nodes, facilitating image segmentation and assessment of tumor heterogeneity, thereby offering more predictive information [43]. Additionally, selecting the peak phase based on the DCE-MRI enhancement time-intensity curve helps to better standardize the study methodology [44].

To extract more information from the primary lesion, previous studies on predicting NAT response extended the primary lesion automatically by four millimeters [45] but did not analyze the lymph node regions in patients who had already undergone SLN. In this study, we enhanced the final Com-RS AUC to 0.918 by supplementing the training with features of the SLN and incorporating intertumoral and peritumoral characteristics. Additionally, we compared the predictive values of the primary lesion and the SLN for NAT response. We found that the RS-Primary derived from the primary lesion showed higher prediction capabilities in terms of AUC

and accuracy compared with RS-SLN. The DeLong and LRT test results indicate that the inclusion of SLNs provided additional supplementary information, suggesting that SLNs contain valuable information related to predicting the response to NAT treatment. A total of 7 and 3 most important features were selected from the primary tumor and SLN, respectively. Most selected features (9 of 10) belong to the textural features. This indicates that the heterogeneity within both the primary tumor and SLN were related strongly to the therapeutic efficiency in BC.

Studies have shown that the axillary SLN receives about 70% of the lymphatic drainage from BC [46], and it is an essential prognostic factor for BC, influencing treatment decisions [47]. Research [48] has also indicated that there may be receptor (ER, PR, HER2) discordance between the core needle biopsy tissue of the primary tumor and the axillary SLN. One explanation [49] for receptor changes between the axillary SLN and the primary tumor is the clonal selection hypothesis, which posits that the primary tumor consists of multiple clonal subpopulations capable of metastasis, leading to different tumor cell phenotypes. This demonstrates the heterogeneity between the primary tumor and axillary SLN, suggesting that there may be supplementary information between them. Therefore, by combining the most important features from both the primary tumor and the SLN, the developed RS-Com achieved better prediction performance in terms of AUC and ACC. Our RS-Com was validated with an external cohort and generated consistent results, which may suggest good potential of the RS-Com as a new biomarker to contribute to identifying

Table 4 Performance of the established RSs based on primary lesion and SLN, and their combination for HER2-positive and HER2-negative subtypes

Subtypes	Model	Training cohort				Validation cohort				Test cohort			
		AUC (95% CI)	ACC	SEN	SPE	AUC (95% CI)	ACC	SEN	SPE	AUC (95% CI)	ACC	SEN	SPE
HER2+	RS-Primary	0.721 (0.702–0.781)	0.710	0.735	0.691	0.714 (0.681–0.734)	0.653	0.683	0.801	0.709 (0.653–0.777)	0.653	0.645	0.760
	RS-SLN	0.700 (0.610–0.761)	0.661	0.633	0.740	0.691 (0.582–0.804)	0.591	0.739	0.610	0.683 (0.571–0.810)	0.602	0.619	0.896
	RS-Com	0.812 (0.720–0.891)	0.833	0.891	0.705	0.801 (0.710–0.903)	0.783	0.729	0.842	0.780 (0.631–0.871)	0.730	0.619	0.845
HER2-	RS-Primary	0.719 (0.640–0.877)	0.690	0.702	0.679	0.710 (0.654–0.812)	0.652	0.680	0.792	0.704 (0.581–0.822)	0.634	0.620	0.770
	RS-SLN	0.703 (0.621–0.802)	0.682	0.610	0.733	0.687 (0.565–0.780)	0.581	0.742	0.589	0.669 (0.591–0.820)	0.621	0.602	0.798
	RS-Com	0.782 (0.692–0.901)	0.811	0.831	0.693	0.781 (0.621–0.904)	0.762	0.710	0.862	0.776 (0.672–0.892)	0.734	0.608	0.831

AUC, area under the receiver operating characteristic curve; CI, confidence interval; ACC, accuracy; SEN, sensitivity; SPE, specificity; SLN, suspicious lymph node

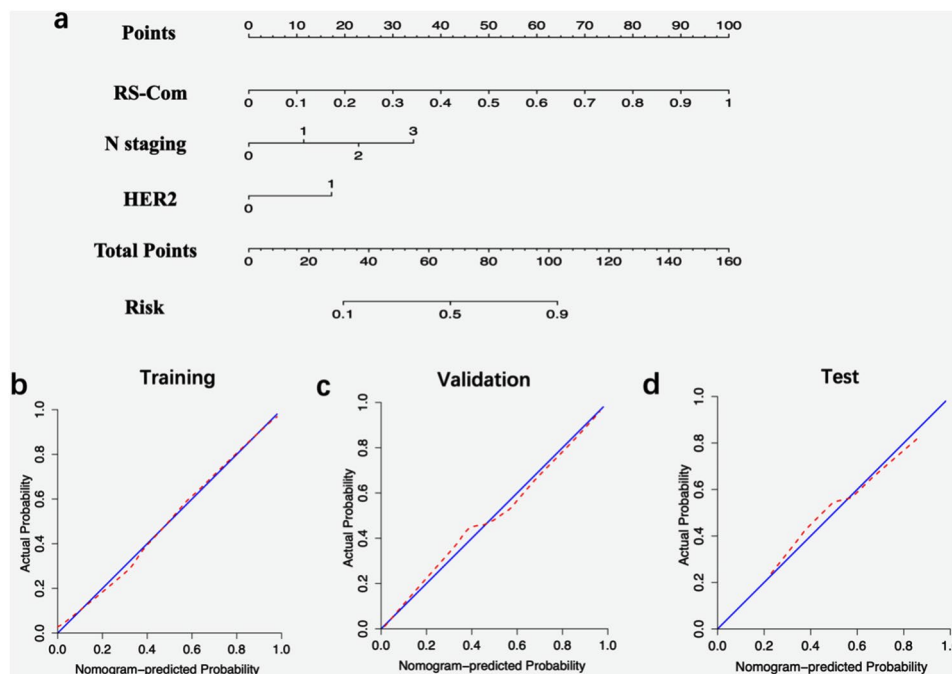


Fig. 5 The clinical-radiomics nomogram integrating RS-Coms, N staging and HER2 for assessing the efficacy of NAT. **(a)** Nomogram. **(b)**, **(c)** and **(d)** Calibration curve analyses of the nomogram in training **(b)**, validation **(c)** and test **(d)** sets

patients who are more likely to benefit from NAT. In the subgroup analysis for HER2-positive and HER2-negative patients, we found that the RS-Com demonstrated a stronger ability to distinguish between effective and ineffective responses to NAT in HER2-positive BC patients. This may be due to the more predictable and consistent response of HER2-positive tumors to targeted therapy, as these tumors exhibit unique imaging features related to treatment outcomes, making it easier for the model to identify treatment responses [50].

Previous works [51, 52] have demonstrated that ER status, PR status, HER2 status, Ki-67, and axillary lymph node status are powerful independent predictors of patient response (MP4-5), suggesting that NAT-high response may be related to these indicators, particularly the grading of HER2 and axillary SLN. Since HER2 receptor-positive targeted drugs were incorporated into neoadjuvant chemotherapy regimens, especially the use of epratuzumab in conjunction with trastuzumab, the efficacy of NAT in patients has significantly improved [53]. Similarly, a meta-analysis [54] has shown that HER2 is an independent predictor of axillary lymph node response to neoadjuvant chemotherapy. Therefore, in this experiment, incorporating HER2 and N stage as effective clinical indicators enhanced the predictive performance of the nomogram for NAT response. The nomogram

developed in this study can better assist clinicians in predicting patient response to NAT.

The limitations of the study are evident in several aspects. Firstly, the use of a small patient sample and a retrospective study design introduces the possibility of patient selection bias, which could affect the generalizability of the findings. To strengthen the validity of the results, it would be beneficial to conduct a more extensive study involving a larger number of patients from multiple centers. Secondly, the experiment was performed with a single MRI sequence, the inclusion of multiple MRI sequences could provide a more comprehensive understanding of the imaging characteristics and enhance the robustness of the study. Thirdly, this investigation involves the suspicious axillary lymph nodes on the same side as the primary lesion, which are identified through clinical diagnosis rather than confirmed as metastatic lymph nodes by biopsy. Fourth, future work could integrate longitudinal imaging data from multiple time points to further improve model performance. Fifth, future experiments could develop models to predict ypT0/Tis ypN0 and identify pathological lymph node-negative cases in patients with clinically positive lymph nodes. Lastly, most of the selected features were high-dimensional features, which results in lack of a clear biological explanation for the features and their variations poses a challenge in terms of interpretability.

Table 5 Comparison of the RS-Com, clinical model, and nomogram

Model	Training cohort			P	Validation cohort			P	Test cohort			P
	AUC (95% CI)	ACC	SPE		AUC (95% CI)	ACC	SPE		AUC (95% CI)	ACC	SPE	
Nomogram	0.926 (0.881-0.972)	0.859	0.914	0.814	0.868 (0.778-0.958)	0.766	0.724	0.914	0.839 (0.691-0.988)	0.733	0.857	0.750
Clinical Model	0.698 (0.609-0.786)	0.602	0.586	0.757	0.694 (0.557-0.820)	0.625	0.621	0.686	0.663 (0.530-0.856)	0.567	0.786	0.563
RS-Com	0.918 (0.873-0.964)	0.815	0.931	0.757	0.822 (0.712-0.932)	0.781	0.759	0.857	0.817 (0.662-0.972)	0.733	0.946	0.625
Nomogram vs. Clinical Model				<0.001*								0.032*
RS-Com vs. Nomogram				0.004*								<0.001*
RS-Com vs. Clinical Model				0.331								0.165

AUC, area under the receiver operating characteristic curve; CI, confidence interval; ACC, accuracy; SEN, sensitivity; SPE, specificity

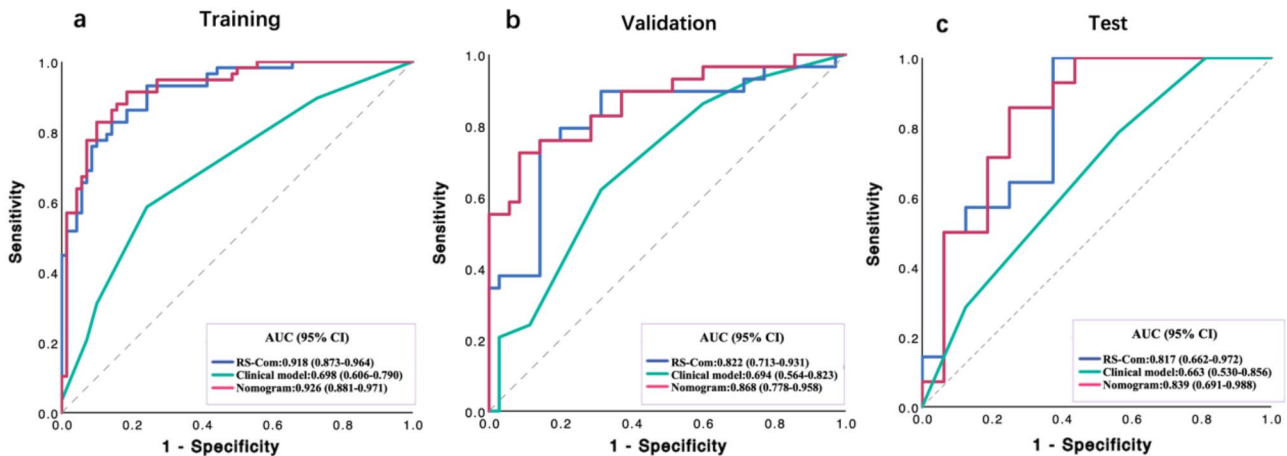


Fig. 6 ROC curves of the nomogram, clinical model and RS-Com in training (a), validation (b) and test (c) sets

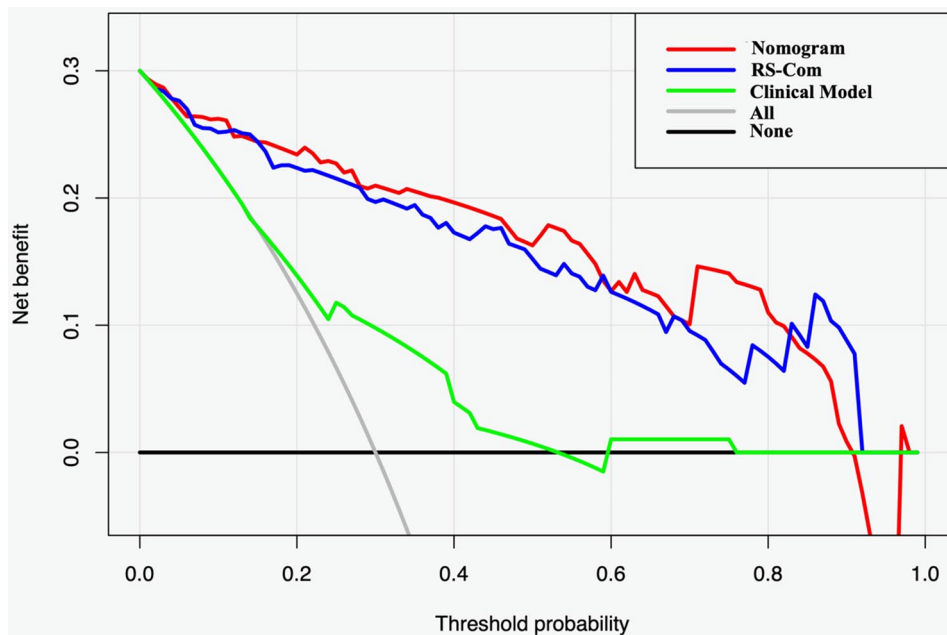


Fig. 7 Decision curve analyses of the nomogram, RS-Com and clinical model. X-axis and y-axis showed the threshold probability and net benefit, respectively. The red, blue, and green lines represent decisions made by the nomogram, clinical model and RS-Com, respectively. The black line represents the assumption that all patients were NAT-low and not treated, whereas the gray line represents the hypothesis that all patients are NAT-high and received treatment

Conclusion

Features from SLN can provide supplementary information to the primary BC. The nomogram developed in conjunction with N staging and HER2 can effectively predict response to NAT and may assist clinicians in making individual treatment decisions for patients with BC.

Abbreviations

- AIC Akaike information criterion
- AJCC American Joint Committee on Cancer
- AUC Area under the curve
- BC Breast cancer
- DCA Decision curve analyses
- DCE-MRI Dynamic contrast-enhanced magnetic resonance imaging

- ER Estrogen receptor
- HER2 Human Epidermal Growth Factor Receptor
- ICC Inter-class correlation coefficient
- LASSO Least absolute shrinkage and selection operator
- MP Miller-Payne
- NAT Neoadjuvant therapy
- PR Progesterone receptor
- RCB Residual Cancer Burden
- ROC Receiver operating characteristic
- ROI Regions of interest
- RS Radiomic signature
- SD Standard deviation
- SLN Suspicious lymph node
- VIF Variance inflation factor

Supplementary Information

The online version contains supplementary material available at <https://doi.org/10.1186/s12885-025-14004-3>.

Supplementary Material 1

Acknowledgements

The study was supported by Climbing Fund of National Cancer Center (NCC201906B01) and Shenyang Key Laboratory of Advanced Medical Imaging System Technology (19-110-4-10).

Author contributions

D.Z. and Y.Y.S. contributed to study concepts and manuscript preparation. D.Z., Y.Y.S. and Q.X.L. contributed to study design. Q.X.L., Y.Q.D. and Y.Y.S. contributed to data acquisition. Y.Y.S., Q.X.L. and Y.F. contributed to quality control of data and algorithms. C.X.C., C.N.Y., Y.Y.S. and Q.X.L. contributed to data analysis and interpretation. Y.Y.S. contributed to statistical analysis. Y.Y.S., D.Z., Y.F. and Y.H. contributed to manuscript review. All authors read and approved the final manuscript.

Funding

The study was supported by Climbing Fund of National Cancer Center (NCC201906B01) and Shenyang Key Laboratory of Advanced Medical Imaging System Technology (19-110-4-10).

Data availability

The datasets used and/or analyzed during the current study are available from the corresponding author upon reasonable request.

Declarations

Ethics approval and consent to participate

This retrospective analysis was approved by the Ethics Committee of Liaoning Cancer Hospital, affiliated with Liaoning Cancer Hospital (Approval No. [20221101]), and the Ethics Committee of the Affiliated Hospital of Qingdao University, affiliated with Qingdao University (Approval No. [QYFY WZLL 28631]), with a waiver of written informed consent from the institutional review board.

Consent for publication

Not applicable.

Competing interests

The authors declare no competing interests.

Received: 14 October 2024 / Accepted: 24 March 2025

Published online: 01 April 2025

References

- Sung H, Ferlay J, Siegel RL, Laversanne M, Soerjomataram I, Jemal A, Bray F. Global cancer statistics 2020: GLOBOCAN estimates of incidence and mortality worldwide for 36 cancers in 185 countries. *Ca-Cancer J Clin*. 2021;71(3):209–49.
- Song DL, Yang F, Zhang YJ, Guo YZ, Qu YW, Zhang XC, Zhu YX, Cui SJ. Dynamic contrast-enhanced MRI radiomics nomogram for predicting axillary lymph node metastasis in breast cancer. *Cancer Imaging*. 2022;22(1).
- Thompson AM, Moulder-Thompson SL. Neoadjuvant treatment of breast cancer. *Ann Oncol*. 2012;23:231–6.
- Korde LA, Somerfield MR, Carey LA, Crews JR, Denduluri N, Hwang ES, Khan SA, Loibl S, Morris EA, Perez A, et al. Neoadjuvant chemotherapy, endocrine therapy, and targeted therapy for breast cancer: ASCO guideline. *J Clin Oncol*. 2021;39(13):1485–505.
- Ogston KN, Miller ID, Payne S, Hutcheon AW, Sarkar TK, Smith I, Schofield A, Heys SD. A new histological grading system to assess response of breast cancers to primary chemotherapy: prognostic significance and survival. *Breast*. 2003;12(5):320–7.
- Symmans WF, Peintinger F, Hatzis C, Rajan R, Kuerer H, Valero V, Assad L, Poniecka A, Hennessy B, Green M, et al. Measurement of residual breast cancer burden to predict survival after neoadjuvant chemotherapy. *J Clin Oncol*. 2007;25(28):4414–22.
- Yee D, DeMichele AM, Yau C, Isaacs C, Symmans WF, Albain KS, Chen YY, Krings G, Wei S, Harada S, et al. Association of Event-Free and distant Recurrence-Free survival with Individual-Level pathologic complete response in neoadjuvant treatment of stages 2 and 3 breast cancer Three-Year Follow-up analysis for the I-SPY2 adaptively randomized clinical trial. *Jama Oncol*. 2020;6(9):1355–62.
- Cortazar P, Zhang L, Untch M. Pathological complete response and long-term clinical benefit in breast cancer: the CTNeoBC pooled analysis (384, Pg 164, 2014). *Lancet*. 2019;393(10175):986–986.
- Zhang MQ, Du Y, Zha HL, Liu XP, Cai MJ, Chen ZH, Chen R, Wang J, Wang SJ, Zhang JL et al. Construction and validation of a personalized nomogram of ultrasound for pretreatment prediction of breast cancer patients sensitive to neoadjuvant chemotherapy. *Brit J Radiol*. 2022;95(1140).
- Chen S, Liu Y, Ouyang QW, Huang L, Luo RC, Shao ZM. Clinical and pathological response to neoadjuvant chemotherapy based on primary tumor reduction is correlated to survival in hormone Receptor-Positive but not hormone Receptor-Negative locally advanced breast cancer. *Ann Surg Oncol*. 2015;22(1):32–9.
- Lambin P, Rios-Velazquez E, Leijenaar R, Carvalho S, van Stiphout RG, Granton P, Zegers CM, Gillies R, Boellard R, Dekker A, et al. Radiomics: extracting more information from medical images using advanced feature analysis. *Eur J Cancer (Oxford England: 1990)*. 2012;48(4):441–6.
- Cain EH, Saha A, Harowicz MR, Marks JR, Marcom PK, Mazurowski MA. Multivariate machine learning models for prediction of pathologic response to neoadjuvant therapy in breast cancer using MRI features: a study using an independent validation set. *Breast Cancer Res Tr*. 2019;173(2):455–63.
- Xu ML, Yang HM, Sun J, Hao HF, Li XJ, Liu GF. Development of an intratumoral and peritumoral radiomics nomogram using digital breast tomosynthesis for preoperative assessment of lymphovascular invasion in invasive breast cancer. *Acad Radiol*. 2024;31(5):1748–61.
- Guo W, Li H, Zhu Y, Lan L, Yang S, Drukker K, Morris E, Burnside E, Whitman G, Giger ML, et al. Prediction of clinical phenotypes in invasive breast carcinomas from the integration of radiomics and genomics data. *J Med Imaging (Bellingham Wash)*. 2015;2(4):041007.
- Agner SC, Rosen MA, Englander S, Tomaszewski JE, Feldman MD, Zhang P, Mies C, Schnall MD, Madabhushi A. Computerized image analysis for identifying Triple-Negative breast cancers and differentiating them from other molecular subtypes of breast cancer on dynamic Contrast-enhanced MR images: A feasibility study. *Radiology*. 2014;272(1):91–9.
- Zhu YT, Li H, Guo WT, Drukker K, Lan L, Giger ML, Ji Y. Deciphering genomic underpinnings of quantitative MRI-based radiomic phenotypes of invasive breast carcinoma. *Sci Rep-Uk*. 2015;5.
- Fan M, Chen H, You C, Liu L, Gu YJ, Peng WJ, Gao X, Li LH. Radiomics of tumor heterogeneity in longitudinal dynamic Contrast-Enhanced magnetic resonance imaging for predicting response to neoadjuvant chemotherapy in breast cancer. *Front Mol Biosci*. 2021;8.
- Wang J, Kato F, Oyama-Manabe N, Li RJ, Cui Y, Tha KK, Yamashita H, Kudo K, Shirato H. Identifying Triple-Negative breast cancer using background parenchymal enhancement heterogeneity on dynamic Contrast-Enhanced MRI: A pilot radiomics study. *PLoS ONE*. 2015;10(11).
- Lee H-j, Lee JH, Lee JE, Na YM, Park MH, Lee JS, Lim HS. Prediction of early clinical response to neoadjuvant chemotherapy in Triple-negative breast cancer: incorporating radiomics through breast MRI. *Sci Rep*. 2024;14(1):21691.
- Liang X, Yu X, Gao T. Machine learning with magnetic resonance imaging for prediction of response to neoadjuvant chemotherapy in breast cancer: A systematic review and meta-analysis. *Eur J Radiol*. 2022;150:110247.
- Joo S, Ko ES, Kwon S, Jeon E, Jung H, Kim J-Y, Chung MJ, Im Y-H. Multimodal deep learning models for the prediction of pathologic response to neoadjuvant chemotherapy in breast cancer. *Sci Rep*. 2021;11(1):18800.
- Locopo N, Fanelli M, Gasparini G. Clinical significance of angiogenic factors in breast cancer. *Breast Cancer Res Treat*. 1998;52(1–3):159–73.
- Conklin MW, Keely PJ. Why the stroma matters in breast cancer insights into breast cancer patient outcomes through the examination of stromal biomarkers. *Cell Adhes Migr*. 2012;6(3):249–60.
- Christiansen A, Detmar M. Lymphangiogenesis and cancer. *Genes cancer*. 2011;2(12):1146–58.
- Mohammed ZM, McMillan DC, Edwards J, Mallon E, Doughty JC, Orange C, Going JJ. The relationship between lymphovascular invasion and

- angiogenesis, hormone receptors, cell proliferation and survival in patients with primary operable invasive ductal breast cancer. *BMC Clin Pathol.* 2013;13(1):31.
26. Sanchez-Munoz A, Navarro-Perez V, Plata-Fernandez Y, Santonja A, Moreno I, Ribelles N, Alba E. Proliferation determined by Ki-67 defines different pathologic response to neoadjuvant Trastuzumab-Based chemotherapy in HER2-Positive breast cancer. *Clin Breast Cancer.* 2015;15(5):343–7.
 27. Greco M, Crippa F, Agresti R, Seregini E, Gerali A, Giovanazzi R, Micheli A, Asero S, Ferraris C, Gennaro M. Axillary lymph node staging in breast cancer by 2-fluoro-2-deoxy-D-glucose-positron emission tomography: clinical evaluation and alternative management. *J Natl Cancer Inst.* 2001;93(8):630–5.
 28. Mittendorf EA, Hunt KK, Boughey JC, Bassett R, Degnim AC, Harrell R, Yi M, Meric-Bernstam F, Ross MI, Babiera GV. Incorporation of Sentinel lymph node metastasis size into a nomogram predicting nonsentinel lymph node involvement in breast cancer patients with a positive Sentinel lymph node. *Ann Surg.* 2012;255(1):109–15.
 29. Ding J, Chen S, Serrano Sosa M, Cattell R, Lei L, Sun J, Prasanna P, Liu C, Huang C. Optimizing the peritumoral region size in radiomics analysis for Sentinel lymph node status prediction in breast cancer. *Acad Radiol.* 2022;29(Suppl 1):S223–8.
 30. van Griethuysen JJM, Fedorov A, Parmar C, Hosny A, Aucoin N, Narayan V, Beets-Tan RGH, Fillion-Robin JC, Pieper S, Aerts H. Computational radiomics system to Decode the radiographic phenotype. *Cancer Res.* 2017;77(21):e104–7.
 31. Gu Z, Huang J, Zhou C, Wang Q, Kong J, You X, Zhang Z, Zhao H. Assessing breast cancer volume alterations post-neoadjuvant chemotherapy through DenseNet-201 deep learning analysis on DCE-MRI. *J Radiation Res Appl Sci.* 2024;17(3):100971.
 32. Koo TK, Li MY. A guideline of selecting and reporting intraclass correlation coefficients for reliability research. *J Chiropr Med.* 2016;15(2):155–63.
 33. Tuv E, Borisov A, Runger G, Torkkola K. Feature selection with ensembles, artificial variables, and redundancy elimination. *J Mach Learn Res.* 2009;10:1341–66.
 34. Pan W. Akaike's information criterion in generalized estimating equations. *Biometrics.* 2001;57(1):120–5.
 35. Xue C, Yuan J, Lo GG, Chang AT, Poon DM, Wong OL, Zhou Y, Chu WC. Radiomics feature reliability assessed by intraclass correlation coefficient: a systematic review. *Quant Imaging Med Surg.* 2021;11(10):4431.
 36. Iasonos A, Schrag D, Raj GV, Panageas KS. How to build and interpret a nomogram for cancer prognosis. *J Clin Oncol.* 2008;26(8):1364–70.
 37. Ruopp MD, Perkins NJ, Whitcomb BW, Schisterman EF. Youden index and optimal cut-point estimated from observations affected by a lower limit of detection. *Biometrical J.* 2008;50(3):419–30.
 38. Molodianovitch K, Faraggi D, Reiser B. Comparing the areas under two correlated ROC curves: parametric and non-parametric approaches. *Biometrical J.* 2006;48(5):745–57.
 39. Zhang D, Zhang B. Semiparametric empirical likelihood confidence intervals for the difference of areas under two correlated ROC curves under density ratio model. *Biom J.* 2014;56(4):678–96.
 40. Liu J, Sun D, Chen L, Fang Z, Song W, Guo D, Ni T, Liu C, Feng L, Xia Y, et al. Radiomics analysis of dynamic Contrast-Enhanced magnetic resonance imaging for the prediction of Sentinel lymph node metastasis in breast cancer. *Front Oncol.* 2019;9:980.
 41. Marinovich ML, Sardaneli F, Ciatto S, Mamounas E, Brennan M, Macaskill P, Irwig L, von Minckwitz G, Houssami N. Early prediction of pathologic response to neoadjuvant therapy in breast cancer: systematic review of the accuracy of MRI. *Breast.* 2012;21(5):669–77.
 42. Delille JP, Slaneta PJ, Yeh ED, Halpern EF, Kopans DB, Garrido L. Invasive ductal breast carcinoma response to neoadjuvant chemotherapy: noninvasive monitoring with functional MR imaging - Pilot study. *Radiology.* 2003;228(1):63–9.
 43. Romeo V. Standardization of quantitative DCE-MRI parameters measurement: an urgent need for breast cancer imaging. *Acad Radiol.* 2022;29(Suppl 1):S87–8.
 44. Chang RF, Chen HH, Chang YC, Huang CS, Chen JH, Lo CM. Quantification of breast tumor heterogeneity for ER status, HER2 status, and TN molecular subtype evaluation on DCE-MRI. *Magn Reson Imaging.* 2016;34(6):809–19.
 45. Niu SX, Jiang WY, Zhao NN, Jiang T, Dong Y, Luo YH, Yu T, Jiang XR. Intra- and peritumoral radiomics on assessment of breast cancer molecular subtypes based on mammography and MRI. *J Cancer Res Clin.* 2022;148(1):97–106.
 46. Ocaña A, Diez-González L, Adrover E, Fernández-Aramburo A, Pandiella A, Amir E. Tumor-infiltrating lymphocytes in breast cancer: ready for prime time? *J Clin Oncol.* 2015;33(11):1298–9.
 47. Tamirisa N, Thomas SM, Fayanzu OM, Greenup RA, Rosenberger LH, Hyslop T, Hwang ES, Plichta JK. Axillary nodal evaluation in elderly breast cancer patients: potential effects on treatment decisions and survival. *Ann Surg Oncol.* 2018;25(10):2890–8.
 48. Weydandt L, Nel I, Kreklau A, Horn LC, Aktas B. Heterogeneity between core needle biopsy and synchronous axillary lymph node metastases in early breast cancer Patients-A comparison of HER2, Estrogen and progesterone receptor expression profiles during primary treatment regime. *Cancers.* 2022;14(8).
 49. Almendro V, Fuster G. Heterogeneity of breast cancer: etiology and clinical relevance. *Clin Transl Oncol.* 2011;13(11):767–73.
 50. Brasó-Maristany F, Griguolo G, Pascual T, Paré L, Nuciforo P, Llombart-Cussac A, Bermejo B, Oliveira M, Morales S, Martínez N. Phenotypic changes of HER2-positive breast cancer during and after dual HER2 Blockade. *Nat Commun.* 2020;11(1):385.
 51. Gu J, Tong T, He C, Xu M, Yang X, Tian J, Jiang T, Wang K. Deep learning radiomics of ultrasonography can predict response to neoadjuvant chemotherapy in breast cancer at an early stage of treatment: a prospective study. *Eur Radiol.* 2022;32(3):2099–109.
 52. Wang XL, Hua H, Han JQ, Zhong X, Liu JJ, Chen JJ. Evaluation of multiparametric MRI Radiomics-Based nomogram in prediction of response to neoadjuvant chemotherapy in breast cancer: A Two-Center study. *Clin Breast Cancer.* 2023;23(6):e331–44.
 53. Tolaney SM, Barry WT, Dang CT, Yardley DA, Moy B, Marcom PK, Albain KS, Rugo HS, Ellis M, Shapira I, et al. Adjuvant Paclitaxel and trastuzumab for Node-Negative, HER2-Positive breast cancer. *New Engl J Med.* 2015;372(2):134–41.
 54. Samiei S, Simons JM, Engelen SME, Beets-Tan RGH, Classe JM, Smidt ML, Grp E. Axillary pathologic complete response after neoadjuvant systemic therapy by breast cancer subtype in patients with initially clinically Node-Positive disease A systematic review and Meta-analysis. *Jama Surg.* 2021;156(6).

Publisher's note

Springer Nature remains neutral with regard to jurisdictional claims in published maps and institutional affiliations.